Bayesian statistical analysis of ground-clutter for the relative calibration of dual polarization weather radars

Article *in* European Journal of Remote Sensing · December 2016

DOI: 10.5721/EuJRS20164949

CITATIONS
0

READS
72

3 authors, including:

Marta Tecla Falconi
Sapienza University of Rome
9 PUBLICATIONS **1** CITATION
SEE PROFILE

Mario Montopoli
University of Cambridge
124 PUBLICATIONS **551** CITATIONS
SEE PROFILE

European Journal of Remote Sensing - 2016, 49: 933-953
doi: 10.5721/EuJRS20164949
Received 14/03/2016 accepted 10/10/2016

European Journal of Remote Sensing
An official journal of the Italian Society of Remote Sensing

www.aitjournal.com

Bayesian statistical analysis of ground-clutter for the relative calibration of dual polarization weather radars

Marta Tecla Falconi[1]*, Mario Montopoli[2] and Frank Silvio Marzano[1]

[1]Department of Information Engineering, Electronics and Telecommunications, Sapienza, University of Rome, Via Eudossiana, 18, 00184 - Rome, Italy
[2]National Research Council of Italy, Institute of Atmospheric Science and Climate, Via del Fosso del Cavaliere, 100, 00133 - Rome, Italy
*Corresponding author, e-mail address: falconi@diet.uniroma1.it

Abstract
A new data processing methodology, based on the statistical analysis of ground-clutter echoes and aimed at investigating the stability of the weather radar relative calibration, is presented. A Bayesian classification scheme has been used to identify meteorological and/or ground-clutter echoes. The outcome is evaluated on a training dataset using statistical score indexes through the comparison with a deterministic clutter map. After discriminating the ground clutter areas, we have focused on the spatial analysis of robust and stable returns by using an automated region-merging algorithm. The temporal series of the ground-clutter statistical parameters, extracted from the spatial analysis and expressed in terms of percentile and mean values, have been used to estimate the relative clutter calibration and its uncertainty for both co-polar and differential reflectivity. The proposed methodology has been applied to a dataset collected by a C-band weather radar in southern Italy.

Keywords: Calibration, analysis techniques, radar clutter, Bayes classifier, meteorological radar, radar polarimetry.

Introduction
Ground-based weather radars are typically used to locate precipitation over large areas and classify its type (e.g., rain, snow, hail) as well as quantitatively estimate rain accumulations at the ground level. The outcome of the aforementioned applications is strongly dependent by a proper radar system calibration in both single- and dual-polarization modes, that is, by the exact definition of the radar constants involved when trying to convert the received backscattered power into the co-polar reflectivity (Z_{hh}) and the differential reflectivity (Z_{dr}) in the radar equation. Both Z_{hh} and Z_{dr} are the radar quantities considered to estimate rain precipitation and perform hydrometeor classifications. They are often used together with the specific differential phase shift (K_{dp}) that is not affected by miscalibration effects being a measure of the rate of range variations of the differential signal phase between the horizonatal (h) and vertical polarization (v). It happens that such radar constants (i.e.

transmitted peak power, antenna technical features and in general all the radar transmitter and receiver system parameters) may slightly change over time departing from their nominal values.

Several techniques have been developed to check the degree of calibration of a radar system and compensate for it. For example, Holleman et al. [2010] proposed to observe the incoherent radiation from the Sun as a stable reference to define the level of miscalibrations in the receiver section of the radar systems in terms of Z_{hh}. In Gorgucci et al. [1999], the degree of redundancy shown in the dual polarization radar measurements of Z_{hh}, Z_{dr} and K_{dp}, in light rain regimes, is exploited to find an absolute calibration factor for Z_{hh}. For the Z_{dr} calibration, the same Authors, proposed a vertical looking strategy of rain drops while they fall on the radar. Later, Bringi and Chandrasekar [2001] and Ryzhkov et al. [2005] prosed a theoretical curve relating the vertical looking observations of Z_{dr} to the slanted ones, thus providing an alternative way to find a calibration factor for Z_{dr} that is not limited to the availability of vertical scan only. A third more recent technique proposes the use of ground-clutter signature as reference target to monitor the calibration status of the radar system relatively to a starting time of observation [Silberstein et al., 2008; Wolff et al., 2015; Golbon-Haghighi et al., 2015]. Note that this technique does not provide an absolute calibration factor but, instead, it allow monitoring the system calibration over the time, which is a useful aspect in operational contexts.

It is worth mentioning that there exist other radar calibration methodologies aimed at merging all the aforementioned techniques [e.g., Ice et al., 2014; Falconi et al., 2015; Vaccarono et al., 2016]. The final goal of such blended techniques is to increase the chance to have a more accurate and continuous reference source for calibration. In addition, when multiple source of calibration are took into account all the calibration information can be summarized, for example using a fuzzy logic approach, in a single diagnostic quality index, which can be useful to take decisions on where and when a direct technical intervention is necessary on the radar system [Falconi et al., 2015]. Independently by the calibration method adopted, the typical precision when calibrating Z_{hh} and Z_{dr} is 1 dBZ and 0.1 dB, respectively. These requirements limit the impact of the system error on the estimation of precipitation intensity and on hydrometeor classifications [Bringi and Chandrasekar, 2001] and at the same time poses a severe criterion in the selection and the implementation of the various calibration techniques.

In this work, we want to investigate in more detail the relative calibration technique based on the use of the ground clutter try to put the basis for improving its reliability. In particular, our attention is focused on algorithm aspects for a more robust clutter identification and its spatial categorization to automatically and objectively identify the targeted areas of “best clutter” for a more accurate calibration monitoring based on ground clutter information.

Ground-clutter characteristics, modeling and simulation have been extensively studied by several authors in order to improve the radar detection of meteorological targets [e.g., Hubbert et al., 2009a, 2009b]. In a typical radar processing chain, the ground clutter is usually automatically detected using some specific and well-consolidated algorithms and then rejected to retain only the radar echoes originated by rain precipitation processes. One of the first efforts to discriminate precipitation echoes from ground-clutter was made by Browning [1978] that has analyzed in depth the characteristics of the clear-air radar signal with respect to those related to meteorological targets. Later, with the work of

Moszkowicz et al. [1994] some automated approaches, using established methods like Bayesian classification schemes, have been applied for the identification of the anomalous propagation and then to ground clutter being the two issues potentially related.
More recently, with the increasing of the computation power, machine-learning techniques including those based on fuzzy logic or neural networks approaches, become more popular. In particular, neural networks and fuzzy logic have been using widely [Haykin and Deng, 1991; Jakubiak et al., 1997; Lee et al., 2015] although comparisons with the standard Bayesian classification approaches [Haykin et al., 1991] showed a slight improvement of the latter with respect to the former [Rico-Ramirez and Cluckie, 2008]. It should be mentioned that other methodologies for the separation of ground clutter and meteo-targets made use of decision-tree classifier [Steiner and Smith, 2002] as well as of analysis of the received radar signal in the spectral domain [Passarelli et al., 1981; Alku et al., 2015]. Although out of the scope of this study, it is worth mentioning, as the ground clutter is not the unique source of clutter. Other kind of clutters, like for example those originated by sea, birds, chaff and interference caused by telecommunication devices have been studied as well and there are continuous updates on this topic [e.g., Alku et al., 2015; Saltikoff et al., 2016]. For what concern ground clutter, more recently, is emerging the idea that the ground clutter has not to be considered as a disturb that needs to be necessarily discarded but, instead, its characteristic in time and space can be used as a stable reference for the monitoring of weather radar hardware system [Silberstein et al., 2008; Golbon-Haghighi et al., 2015; Wolff et al., 2015]. Thus, a more accurate statistical analysis of the ground-clutter echoes in terms of their temporally and spatially variations, can be useful to formulate a clutter distribution model that can be used to better define the properties of ground clutter which are needed to perform a relative calibration monitoring with the required precision. The calibration using the clutter medium is already widely applied by several national weather services [Silberstein et al., 2008 Golbon-Haghighi et al., 2015; Wolff et al., 2015], although its operative implementation takes indistinctly into account all the ground clutter scenarios thus not considering its statistical variability in space. Actually, a detailed spatial analysis of the ground-clutter might suggest that there exists "targeted clutter areas" more suitable for a robust implementation of the relative calibration strategy. On the other hand, a temporal analysis of such targeted clutter areas can be a very useful tool to estimate the relative calibration and evaluate its uncertainty. Indeed, the temporal monitoring of the variation of the calibration parameters aims at two goals: *i*) provide a synthetic and intuitive visualization of the relative calibration errors and *ii*) measure the uncertainty on such relative calibration errors using for example a moving window standard deviation on daily basis.
Starting from the aforementioned considerations, this work focuses on the following three aspects: (1) apply a Bayesian classifier to identify the ground-clutter areas more suitable for calibration purposes [Rico-Ramirez and Cluckie, 2008]. A statistical analysis based on score indexes is carried out as well to have a degree of accuracy of the clutter identification performed; (2) present a statistical analysis of the targeted ground clutter areas in terms of Z_{hh} and Z_{dr} by applying an automated region merging algorithm [Nock and Nielsen, 2004]; (3) monitor the ground-clutter probability and cumulative distributions in terms of its statistical moments and specifically the mean and 95th percentile [Silberstein et al., 2008]. To accomplish the objectives proposed in this study, the radar-site of Pettinascura

(Cosenza, Calabria) in south of Italy, which is part of the Italian weather radar network, is considered. This is one of the first work on the characterization of the ground-clutter applied to peculiar Italian complex orography scenario, whose orographic characteristics are dominated by coastlines and mountains [Alberoni et al., 2002; Vulpiani et al., 2012].
This paper is organized follows. In section "Weather-radar relative calibration techniques" we define the overall approach together with the study area and available weather radar data. Section "Ground-clutter Bayesian classification" is devoted to introduce the Bayesian classification and score indexes, whereas section "Ground-clutter spatial analysis and radar calibration" presents the region merging algorithm for ground-clutter spatial analysis and illustrates the results in terms of relative calibrations and uncertainty, based on the ground-clutter reference technique, and comparing it with respect to the well-established radar receiver calibration based on Sun monitoring. Conclusions are drawn in section "Conclusions" where future work is outlined as well.

Weather-radar relative calibration techniques

We present in this section the overall algorithm to analyze the calibration status of a radar system together with the study area considered, the available weather radar data and the system characteristics of the radar used in this work.

Overall algorithm approach

Figure 1 shows the block diagram of the overall approach followed to use ground-clutter for monitoring a weather radar system in terms of its relative calibration. The relative calibration approach follows various steps:

1) The first step is aimed at separating the ground-clutter from the weather signal. A Bayesian classification is applied for this purpose. The output of this procedure is a real-time selection indicating the areas affected by clutter and those where hydrometeors are likely present in terms of probabilistic membership. The set of grid points within the radar domain affected by ground clutter is indicated by D. A training data set extracted from measurements of Mt. Pettinascura radar is used to estimate the a priori and the likelihood probability density functions as detailed after.
2) The second step is generally devoted to the use the clutter signal in the domain D, for monitoring the radar system performances. Two statistical moments of the ground clutter probability distribution, namely the mean value or the 95th percentile, are used to synthesize the information brought by the ground-clutter signature. The choice of consider these two statistical moments instead of the overall clutter distribution is made to have a more stable evaluation as will be clear later on. At this step we apply a ground-clutter spatial analysis based on a region merging approach to select different sub-domains of D (hereafter indicated by D^*). The region merging approach works in statistical terms using the cumulative distributions defined on spatial basis and its aim is to verify if there exists optimal sub domains, D^*, which are more stable in terms of ground-clutter statistical parameters. The stability of the result is then evaluated using the daily temporal standard deviation, by assuming that the value of Z_{hh} or Z_{dr} at the grid points of stable clutter within D^* should not vary significantly. The different results are evaluated using both the mean value and the 95th percentile index of the ground clutter probability distribution.

3) The last step is the numerical estimation of the relative calibration value for both radar observables, i.e. co-polar reflectivity $\Delta Z_{hh}^{D^*}$ and differential reflectivity $\Delta Z_{dr}^{D^*}$, using the most stable region domain D^* derived from the previous step. The daily relative calibration index is computed using the mean value of the two radar observable statistics.

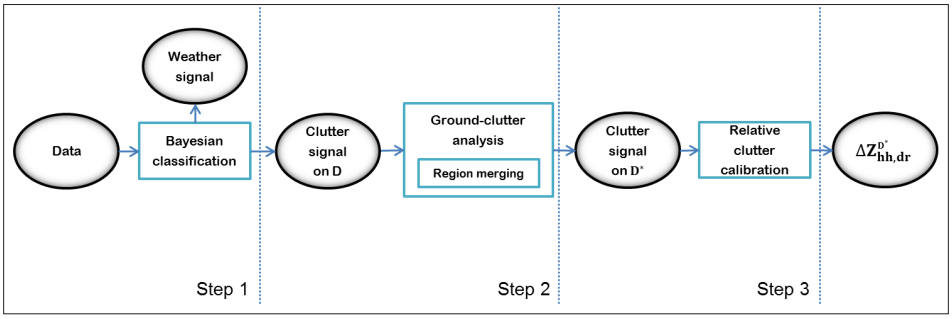

Figure 1 - The overall algorithm to analyze the calibration status of a radar system is shown as detailed in Section "Overall algorithm approach". The block diagram starts with the weather radar data volume and ends in output with the relative calibration results for the co-polar reflectivity and differential reflectivity in the spatial region D*. The sub-domain D* is defined as a stable area in terms of standard deviation of the clutter distribution from the previous ground-clutter analysis as in Section "Ground-clutter analysis by region merging".

System and data

Weather radar network in Italy is mainly used to detect severe weather and related hydro-geological risks. The Italian orography, characterized by small catchments along most coastlines and by the Alpine and Appenine chains, increases the flood hazard especially during the fall season [Alberoni et al., 2002]. In the last years, many extreme rainfall events have highlighted the need of a real time monitoring system. In this scenario the presence of a complex-orography conditions heavily affects the quality of the retrieved radar products and is get more difficult the rain-rate estimation [Vulpiani et al., 2012].

For this study, we have considered the C-band dual polarization radar in southern Italy along the Ionic sea, sited at Mt. Pettinascura (Cosenza, Calabria, Italy). At the basis of this work there is the idea to use the orography as a stable robust reference ("geographical constraint") to estimate the relative radar calibration for the weather radar observables. The location of the radar at about 1705 m and is surrounded by the meridional Appenines and the Sila mountain (Fig. 2). The weather radar exhibits 1° for azimuth resolution as well as 150 and 100 m for the range resolution at slanted and vertical pointing, respectively. The radar system, having Doppler capacity, has different operation modes such as: radar single mode, radar dual h mode, radar dual v mode. The time sampling of the radar scan is 10 minutes and for each sampling time a polar volume, composed by 360° sectors for 11 elevation steps plus a vertical one, is acquired. The radar operates with a nominal wavelength of 5.3 cm and a pulse width, which varies from 1 us until the fourth elevation (3.5°) to 0.5 us until the eleventh elevation (15.99°), and 0.66 us at vertical incidence. This results in a variable range resolution which is sampled at 150; 75; 99 m, respectively.

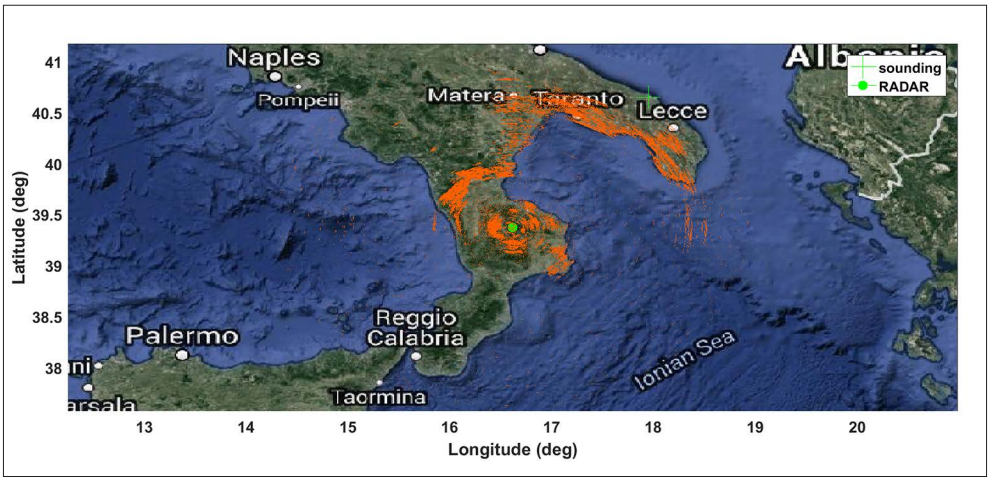

Figure 2 - The clutter mask (red) shows the clutter scenario surround the radar-site of Mt. Pettinascura (green-point), the closest available radiosounding near Brindisi is also shown (green-cross). Background image from: Google Earth.

Table 1 - List of the data-set for the study acquired by the radar-site of Mt. Pettinascura on seven days every 10 minutes (first column). The second two columns present the number of hours in which the acquisition are interested respectively by clear air and meteorological data. The determination of clear-air and precipitation conditions are obtained by using the texture of the differential phase-shift along with a visual inspection of the data. The fourth column shows the freezing-level height (FLH) range as retrieved from the closest available radiosounding of Brindisi (Puglia, Italy) (Radiosonde Database - University of Wyoming), useful information for the Sun monitoring. The last column shows the number of daily acquisition at the first elevation interested by the solar interference.

Date	Clear air periods (UTC)	Meteo periods (UTC)	Freezing Level Height (km)	Sun interference (#)
1 Aug 2014	20:00 – 23:50	00:00 – 20:00	3.6890	1
2 Aug 2014	00:00 – 12:00 15:00 – 22:30	12:00 – 15:00 22:30 – 23:50	4.5045	1
3 Aug 2014	14:00 – 23:50	00:00 – 14:00	4.5640	1
4 Aug 2014	00:00 – 13:00 19:30 – 23:50	13:00 – 19:30	4.2495	2
5 Aug 2014	00:00 – 12:00 22:00 – 23:50	12:00 – 22:00	4.7825	2
6 Aug 2014	-	00:00 – 23:50	3.7800	1
7 Aug 2014	-	00:00 – 23:50	3.8800	1

In this study we have selected the radar data acquired on seven days every 10 min in 2014 from the August 1 until August 7. The events are listed in Table 1 together with the number of hours in clear air and those interested by precipitation and, the freezing-level height (FLH) as

derived from the closest available radiosounding (LIBR, Brindisi Observations (Radiosonde Database - University of Wyoming) and the solar interference (Solar Database - Commission géologique du Canada). The solar interference availability is included in Table 1 as well.

Ground-clutter Bayesian classification

In this section we introduce the Bayesian methodology used to perform the clutter identification. The Bayesian classifier segments the radar polar volume in terms of probabilistic membership for the two classes of meteo and clutter targets. In addition, the score indexes, such as critical success index, the probability of detection and the false alarm rate, are individually analyzed to evaluate the classification performance as well as to find an optimal window size, needed to calculate the input quantities to run the Bayesian classifier. The results are shown separately at the end of this section.

Methodology

The statistical analysis of the observed radar measurements affected by ground clutter is the basis for our study and starts with the ground-clutter Bayesian classification to separate the clutter from the weather signal. The Bayes classifier have to be trained and for this reason we divide the entire data set, described in Table 1, in two parts consisting of a training and a test group of samples. The training data set consists of two days on August 1 and 2, 2014 and it contains both precipitation and clutter echoes whereas the test dataset includes the remaining days. From the training dataset we extracted the likelihood conditional probability distribution functions (PDFs), indicated as $p(\mathbf{x}|c)$, of a set n radar measurement $\mathbf{x}=[x_1, x_2,\ldots, x_n]$ for the class c (c=1 for clutter echoes or c=0 for weather echoes). The term $p(\mathbf{x}|c)$ represents the conditional probability of the input radar measurement, $\mathbf{x}$, given the class c. Note that in general the vector $\mathbf{x}$ can have several number of components although in our case we will limit n to 3 as will be clear later on. The PDFs of the single l-th radar variables, $p(x_l|c)$, are then modelled using the generalized extreme value (GEV) distribution for all the raw radar variables, namely, the co-polar reflectivity, the differential reflectivity, the co-polar correlation coefficient, the differential phase shift, the radial Doppler velocity and the Doppler spectrum width, labelled as Z_{hh}, Z_{dr}, r_{hv}, f_{dp}, V and W, respectively. These distributions are shown in Figure 3 (black and red curves for ground clutter and meteo-targets, respectively) for the training dataset only. Note that for the training dataset, an automatic and more established procedure for the identification of the ground clutter is used. It is based on the properties shown by the texture of the differential phase shift only. A threshold is considered to define a reference ground clutter mask. A further visual inspection analysis is then carried out, using the periods of clear air and ground clutter previously defined in Table 1, to obtain the reference and robust normalized PDFs, shown in Figures 3 and 4. The PDF for the GEV distribution with location parameter μ, scale parameter σ and shape parameter $k\neq0$ is defined as Kotz and Nadarajah [2000]:

$$p\left(x_l\,|c;k;\boldsymbol{\mu};\boldsymbol{\sigma}\right)=\frac{1}{\sigma}exp\left[-\left(1+k\frac{\left(x_l-\boldsymbol{\mu}\right)}{\boldsymbol{\sigma}}\right)^{-\frac{1}{k}}\right]\left(1+k\frac{\left(x_l-\boldsymbol{\mu}\right)}{\boldsymbol{\sigma}}\right)^{-1--\frac{1}{k}} \quad [1]$$

Assuming $(1+k\,(x-\mu)/\sigma) > 0$, the condition $k > 0$ corresponds to the Type II case, while $k < 0$ corresponds to the Type III case whereas $k = 0$ indicates the Type I case. The GEV distributions are introduced in order to implement the naïve Bayes classifier. The term "naïve" is inspired by the fact that the likelihood conditional PDF is not described by a multivariate Gaussian distribution as typically done in Bayesian implementations to simplify the theoretical formulation, but instead, by a product of single normalized PDFs:

$$p\left(\mathbf{x}|c;k,\boldsymbol{\mu},\boldsymbol{\sigma}\right)=\prod_{l=1}^{n} p\left(x_l|c;k,\boldsymbol{\mu},\boldsymbol{\sigma}\right) \quad [2]$$

under the hypothesis that the input radar measurements x_l are independent.
In this study, the naïve Bayesian classifier foresees three input measurements: the standard deviation of differential reflectivity , differential phase-shift and co-polar correlation coefficient [Rico-Ramirez and Cluckie, 2008]. The normalized conditional PDFs, $(x_l|c=1)$ and $(x_l|c=0)$ with l=1, 2, or 3, are shown in Figure 4 for the training dataset of our case of study in black and red curves for ground clutter and meteo-targets, respectively. The normalization is performed with respect to the probability value of the statistical mode of each density distribution. The formulation of the naïve Bayesian classifier assumes that all input measurements are spatially independent and is given by:

$$p\left(\mathrm{c}|\mathbf{x}\right)=\frac{p\left(\mathrm{c}\right)*p\left(\mathbf{X}|c;k,\boldsymbol{\mu},\boldsymbol{\sigma}\right)}{p\left(\mathbf{x}\right)}=\frac{p\left(\mathrm{c}\right)*\prod_{l=1}^{n} p\left(x_l|c;k,\boldsymbol{\mu},\boldsymbol{\sigma}\right)}{\prod_{l=1}^{n} p\left(x_l|c;k,\boldsymbol{\mu},\boldsymbol{\sigma}\right)} \quad [3]$$

where $p(\mathrm{c})$ is the *a-priori* probability of the class c and it is assumed to be the same for clutter and precipitation ($p(c)$=0.5) and $p\left(\mathbf{x}\right)=\prod_{l=1}^{n} p\left(x_l|c;k,\boldsymbol{\mu},\boldsymbol{\sigma}\right)$ under the assumption of independent radar variables. The classification result is obtained using *an* argument-maximum rule (modal value of the PDF) applied on the naïve Bayes metrics for each position $\mathbf{s}=(i,j)$ and each time frame t:

$$\hat{\mathrm{c}}\left(\mathbf{s},t\right)=\underset{\mathrm{c}=0.1}{\operatorname{argmax}}\left[p\left(\mathrm{c}\right)*\prod_{l=1}^{3} p\left(x_l\left(\mathbf{s},t\right)|c\right)\right] \quad [4]$$

where we introduced the space and time dependency and the predicted class $\hat{\mathrm{c}}\left(\mathbf{s},t\right)$ corresponds to the highest posterior probability. Note that when applying Equation [4] on actual radar measurements, the input quantity $x_l(\mathbf{s},t)$ is dynamically evaluated for each time frame on moving windows covering the whole radar domain and centered, at each visiting step, on positions $\mathbf{s}$. It is worth mentioning that the Bayes classifier is strictly dependent on these spatial-moving windows size applied. To define the optimal size of these windows we have used an optimization step using the score indexes as we will discuss in more detail in the following section. Another aspect to highlight in Equation [4] is that while the term $x_l(\mathbf{s},t)$ is dynamically updated at each time step, the conditional probability functions, p, are fixed and defined from the analysis of the training dataset.
At the end of the Bayesian procedure, once defined the terms $p(c)$ and $p(\mathbf{x}|c)$ on a training

dataset, we have two dynamical maps $\left(M_{\hat{c}}\right)$ corresponding to the clutter $\left(\hat{c}=1\right)$ and to the weather signal $\left(\hat{c}=0\right)$, respectively:

$$M_{\hat{c}}\left(\mathbf{s},t\right)=\mathrm{U}_{\mathbf{s}}\hat{c}\left(\mathbf{s}\right)\Big|_{\hat{c}} \qquad [5]$$

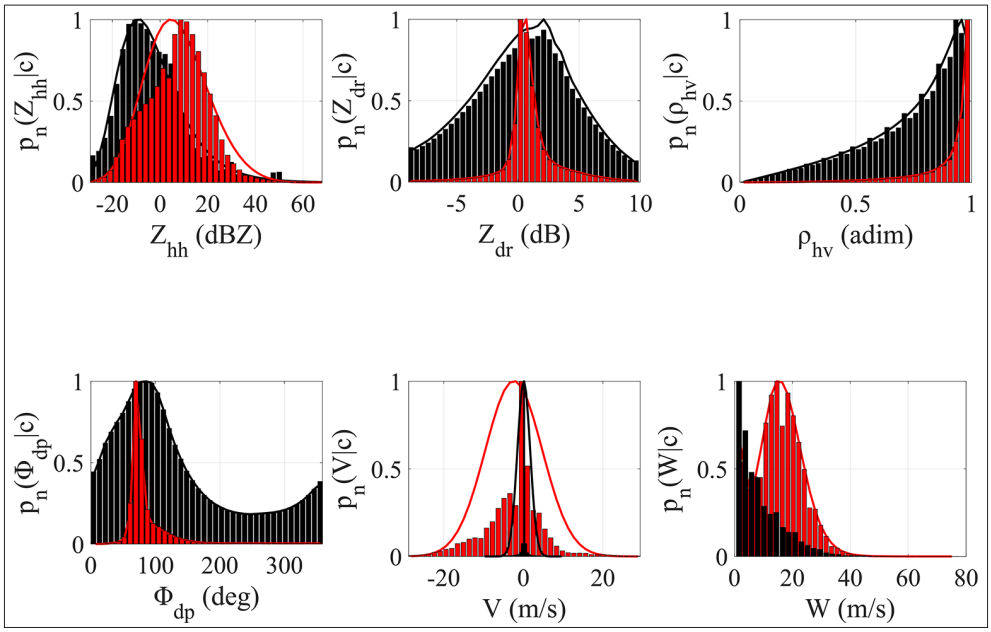

Figure 3 - Normalized spatial and temporal PDFs for precipitation (red) and clutter (black) for the 0.5° elevation, 1 us pulse-length, 750 Hz PRF, 360° scans and 5 rpm obtained on data from 1-2 August. The bars represents the data selected in precipitation (red) and clutter (black), and the line represents the GEV-approximation. The method used to separate precipitation and clutter is a basic filter on the texture of the differential phase improved with the visual inspection of the data.

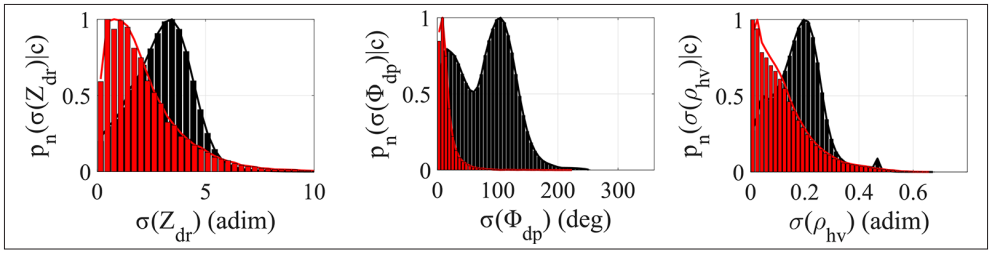

Figure 4 - Precipitation (red) and clutter (black) normalized PDFs at the 0.5 degree elevation for the Bayes classifier, from left the standard deviation of, respectively, differential reflectivity, differential phase shift and co-polar correlation coefficient obtained on data from 1-2 August.

Score indexes and results

The dynamical clutter map obtained for each time frame applying the described Bayes classifier is validated on the test dataset by using some performance indexes, namely: the critical success index (CSI), the probability of detection (POD) and the false alarm rate (FAR) as a measures of classification results. The reference clutter map used as ground-truth for the validation of the Bayes classifier is a deterministic clutter mask obtained with the average of Z_{hh} for one-month of data acquired earlier. The definition of the performance indexes used is [6-8]:

$$\mathrm{CSI} = H / \left(H + M + F\right) \quad [6]$$

$$\mathrm{POD} = H / \left(H + M\right) \quad [7]$$

$$\mathrm{FAR} = F / \left(H + M\right) \quad [8]$$

where H, F, M and C stands for the number of Hit (event observed and predicted), False (event not observed but predicted), Miss (event observed but not predicted) and Correct negatives (event not observed and not predicted).

The CSI score is a valid indicator of the relative worth of different forecast techniques when they are applied to the same environment and is very useful to validate the Bayes classifier [Schaefer, 1990]. We use, as a validation data set, five days on August 3-7, 2014, from the data in Table 1 to calculate the classification performance scores, CSI, POD and FAR resume in Table 2. The indexes are calculated on the entire validation data set, and the resulting values in Table 2 refer to daily means. One of the most critical aspect of the Bayesian classification is the size of the spatial moving windows in which the standard deviation of the input radar variables are calculated (i.e. the $x_i(\mathbf{s},t)$ in Eq. [4]) thus allowing the definition of the probability density functions $(x_i(\mathbf{s},t)|c)$. We have used the performance scores, calculated testing various size of the spatial windows, to set their optimal value. Indeed, the results are shown for three different spatial windows where we can apply the Bayesian classification. The score indexes indicate that the use of a 5x5 spatial window provides the best results for our analysis. Figure 5 shows an example, before and after the Bayesian classification, for a single time step of the analysed event where the proposed Bayesian classifier is able to discriminate between weather signals and ground-clutter even where they appear to be superimposed. This result is significant more better than the common one obtained using a deterministic clutter map [Rico-Ramirez and Cluckie, 2008] where a given grid-point can be classified as ground clutter or as meteo-target without the possibility to quantify the degree of coexistence of the two classes at the same location.

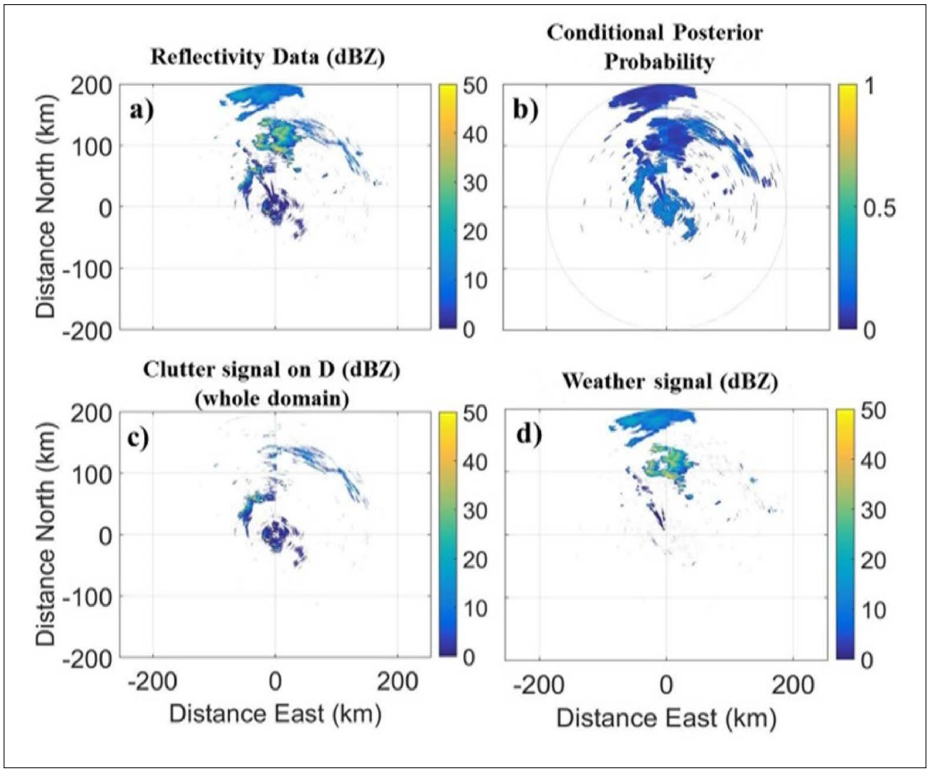

Figure 5 - Case of study of the 5 August 2014 at the 17:10 UTC shown for the co-polar reflectivity Z_{hh} time frame: a) before and c, d) after the application of the Bayesian classification (c for the clutter signal on the whole domain *D* and d for the weather signal); in (b) the conditional posterior probability that is the argument of Equation [4].

Table 2 - By using the deterministic clutter mask as a reference for the dynamical clutter map, obtained from the Bayesian classification, we can see the CSI, POD, FAR results shown in the table for three different windows size. The performance indexes are defined in Section "Score indexes and results" through Equations [6-8]. The spatial-window is the critical parameter for the Bayesian classification and has been tested for three different sizes (3x3; 5x5; 7x7) shown in the first left column of the table. The optimal window correspond to the 5x5 size in which the best performance indexes are obtained.

	3 Aug 2014			4 Aug 2014			5 Aug 2014			6 Aug 2014			7 Aug 2014		
	CSI	POD	FAR	CSI	POD	FAR	CSI	POD	FAR	CSI	POD	FAR	CSI	POD	FAR
3x3	0.79	0.98	0.19	0.87	0.98	0.12	0.84	0.98	0.14	0.79	0.93	0.17	0.85	0.97	0.13
5x5	**0.82**	**0.98**	**0.17**	**0.87**	**0.99**	**0.12**	**0.86**	**0.97**	**0.12**	**0.81**	**0.92**	**0.14**	**0.87**	**0.97**	**0.12**
7x7	0.71	0.99	0.28	0.86	0.99	0.13	0.80	0.99	0.19	0.72	0.97	0.27	0.81	0.99	0.19

Ground-clutter spatial analysis and radar calibration

In this section we first present the formulas for the characterization of ground-clutter relative calibrations. The second part shows the ground-clutter spatial analysis by using the region-merging algorithm in which clutter areas are divided into statistically stable sub-regions that share consistent statistical distributions. Finally, the results of the relative calibration with conventional approaches (i.e. using the whole unpartitioned domain) and the proposed approach (using the statistically-stable sub-regions) are discussed. Note that, as an indirect validation, we also compare the overall proposed approach with the results obtained from the Sun-interference technique.

Characterization of ground-clutter relative calibration

The radar ground-clutter relative calibration can be expressed as the temporal difference between statistical moments of co-polar reflectivity (m_{Zhh}) or differential reflectivity (m_{Zdr}), selected in the whole spatial domain of clutter echoes (indicated by D), between two verification periods at time t and t-1:

$$\Delta m_{Z_x}^{D}(t) = m_{Z_x}^{D}(t) - m_{Z_x}^{D}(t-1) \quad [9]$$

In Equation [9] $m_{Z_x}^{D}(t)$ is a statistical moment of Z_x in the domain D where the subscript "x" stands for "hh" or "dr", indicating the co-polar or the differential reflectivity, respectively. The two moments considered for the ground-clutter characterization are the mean and the 95th percentile: $m_{Z_x}^{D} = \bar{Z}_{Z_x}^{D}$, $m_{Z_x}^{D} = 95Z_x^{D}$, respectively. They are defined as follows:

$$m_{Z_x}^{D} = \begin{cases} 95Z_x^{D}(t) & where \;\; 0.95 = \int_0^{95Z_x^{D}(t)} p\left(Z_x(t)|D\right) dZ_x(t) \\ \bar{Z}_x^{D}(t) & where \;\; \bar{Z}_x^{D}(t) = \int_0^{\infty} Z_x(t)\, p\left(Z_x(t)|D\right) dZ_x \end{cases}$$

We can note that the use of Equation [9] leads to a relative calibration by the difference of value and not to an absolute calibration such as those obtained, for example, by the Sun monitoring. In the next section we will describe how the selection of the clutter domain D can be critical for a meaningful implementation of relative calibration through Equation [9].

Ground-clutter analysis by region merging

After the identification of the domain D (i.e. the set of grid point positions affected by the clutter within the whole radar covered domain) by means of the Bayesian classifier, we can spatially characterize the statistical distributions of Z_{hh} and Z_{dr} affected by ground clutter. However, this is not accomplished in the whole domain D but, instead, in some subdomains of D that need to be automatically and objectively identified, in order to find more stable sub-regions in terms of clutter statistical distribution. This step is important to avoid confusing the fluctuations of the intrinsic clutter echoes (for example due to changes in the state of the vegetation covering the clutter source or to changes linked to environmental factors) with variations that are attributable to the radar system deterioration.

The selection of the sub-domains of D, characterized by a stable ground-clutter PDFs and

labelled as D^*, is objectively accomplished using the region merging algorithm [Nock and Nielsen, 2004]. The region merging algorithm takes in input the dynamical clutter map in the domain D obtained using the Bayes classifier for each time frame within the training dataset and gives as output a subdomain D^* (consisting of sub-regions not necessarily connected each other, i.e. with no intersections). The subdomain D^* has the property to show values of reflectivity with a smaller fluctuation than those in the whole domain D. In a word, the domain D^* is expected to include grid points which show a more stable clutter PDFs. The basic idea of the region merging algorithm is to identify homogeneous ground clutter areas in terms of probability density distributions of $p(x_l(\mathbf{s},t)|c, k, \sigma, \mu)$ defined in Equation [1] where k, σ and μ are the shape, scale and location parameter of a GEV distribution of the radar derived quantity: x_l. The region-merging algorithm follows several steps:

step 1): Select an initial squared sub-region of ground-clutter such that at least 10x10 samples are available and calculate the GEV distribution parameters (shape k, scale σ, and location parameter μ) of $p(x_l(\mathbf{s}, t)|c, k, \sigma, \mu)$ defined in Equation [1];

step 2): Moving the squared sub-region neighboring (with at least 5x5 samples) where we compute its GEV distribution parameters and then their Euclidean distance from the GEV distribution parameters obtained for the first sub-region defined at step 1;

step 3): Impose a tolerance threshold on the Euclidean distance defined at step 2 to decide when two sequential sub-regions must be merged or split. In our case, this threshold is set to 0.5, which we verified to be a good compromise. The sub-regions whose distance is below this tolerance threshold are separated by an edge otherwise they are merged;

step 4): Iterate the steps (2) and (3) till the whole clutter map is completely covered that is, the iterations have explored all spatial domain D.

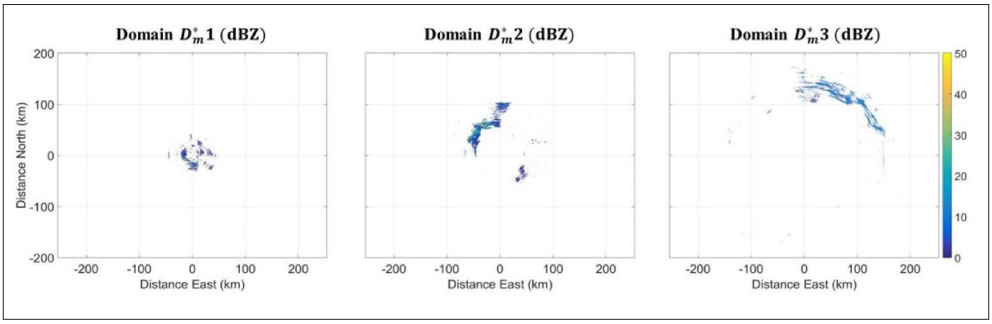

Figure 6 - Case of study of the 5 August 2014 at the 17:10 UTC after the application of the Bayesian classification and region merging in which we obtain three clutter maps (in co-polar reflectivity) for three clutter sub-regions selected on spatial base from left to right: $"D_m^*1"$, $"D_m^*2"$, $"D_m^*3"$, respectively.

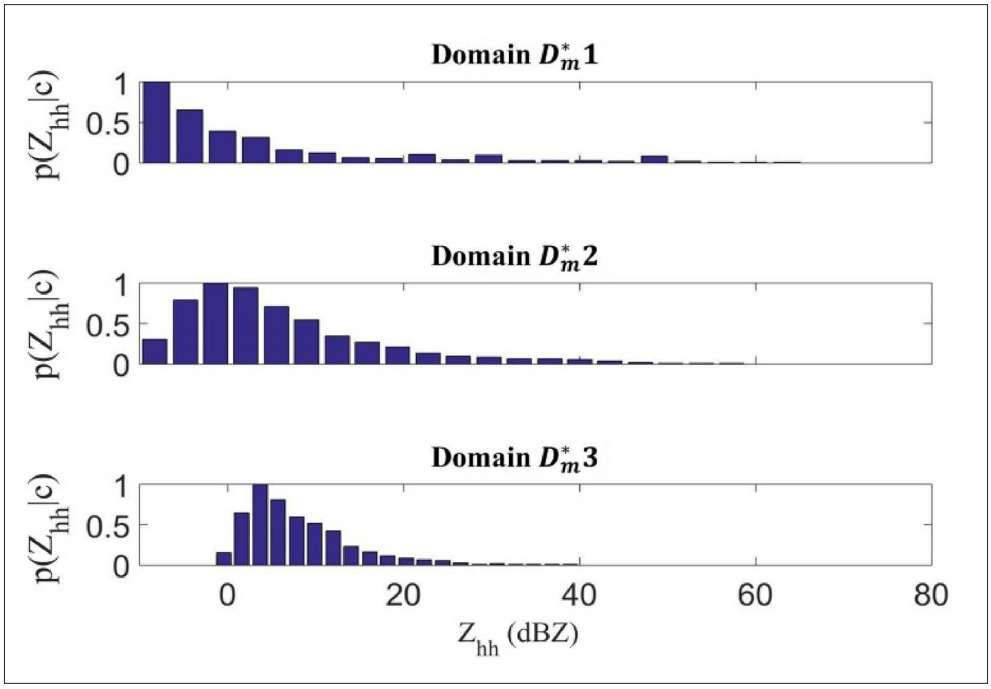

Figure 7 - The normalized PDFs of the three clutter sub-regions selected on spatial base. The parameters of this GEV distributions are shape parameter *k*, scale parameter σ, and the location parameter μ. We can describe the first zone with *k*=0.6837, σ=5.2009, μ=-5.5193, the second zone with *k*=0.1773, σ=7.0187, μ=0.2347 and the last zone with *k*=0.1396, σ=3.8257, μ=4.9951. The results are presented only for the co-polar reflectivity because the region merging shown three stable regions for the co-polar reflectivity and no stable regions for the differential reflectivity.

After the identification of the sub-regions for each analyzed clutter map in the training dataset by running steps 1-4 abovementioned, we identified the minimum clutter sub-regions (D_m^*), which is common to all the available time sequence of the clutter maps.

For our case studies, the region-merging algorithm has identified three different sub-regions or domains: D_m^*1, D_m^*2 *and* D_m^*3. As an example, Figure 6 shows these three domains D_m^*j and j=1, 2 and 3 which are defined considering the data on 3 August 2014 in terms of Z_{hh}, whereas Figure 7 shows the different experimental probability distribution functions for the same regions. The same sub-regions have been tested for the differential reflectivity proving also in this case a more stable trend.

In order to find the domains in D^* which are more stable in terms of clutter statistic of Z_{hh} and Z_{dr} we can analyse the temporal trend of the statistical moments referred to the 95th percentile and the mean values of Z_{hh} and Z_{dr}. They are labelled as $95Z_{hh}^D$ and $95Z_{dr}^D$ and $\bar{Z}_{hh}^D$ and $\bar{Z}_{dr}^D$, respectively where D, in this case, coincides with one of the three domains D_m^*j. The temporal trends of and are shown in Figure 8 whereas those of and are shown in Figure 9. Both figures show also the temporal trends of the statistical moments when the whole domain D is considered.

Reasonably, we can expect the value of each statistical moment in Figures 8 and 9 to be relatively stable on daily basis. Following this consideration, we can identify the areas which

show the more stable clutter signature by looking at the lowest daily standard deviation in each of the $D_m^* j$ domains. In this respect, Tabs. 3-4 show the standard deviation (*s*) of the quantities $\bar{Z}_{hh}^{D_m^* j}$, $\bar{Z}_{dr}^{D_m^* j}$ (in Tab. 3) and $95Z_{hh}^{D_m^* j}$, $95Z_{dr}^{D_m^* j}$ in (in Tab. 4) as well as those referred to the whole domain *D*.

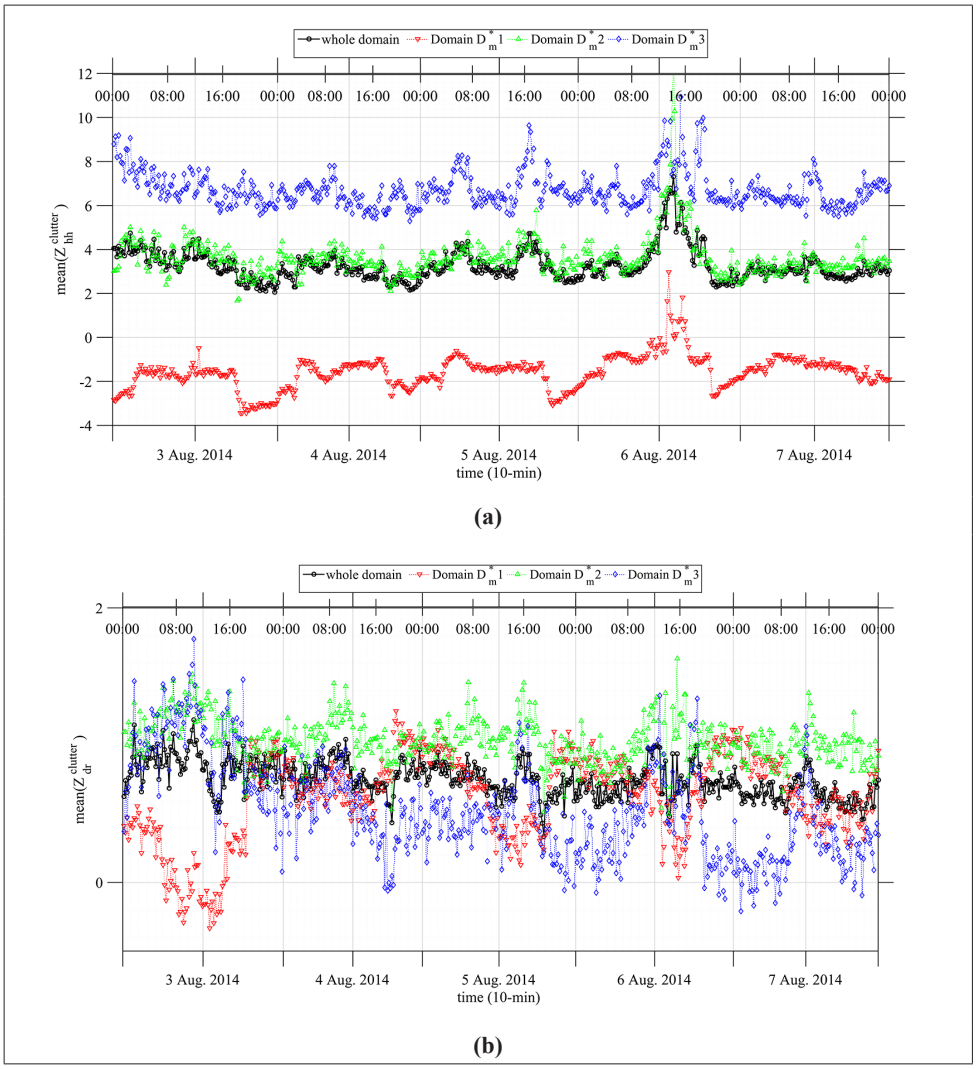

Figure 8 - Temporal trend of acquisition of the mean value of the probability distribution for the co-polar reflectivity (a) and differential reflectivity (b).

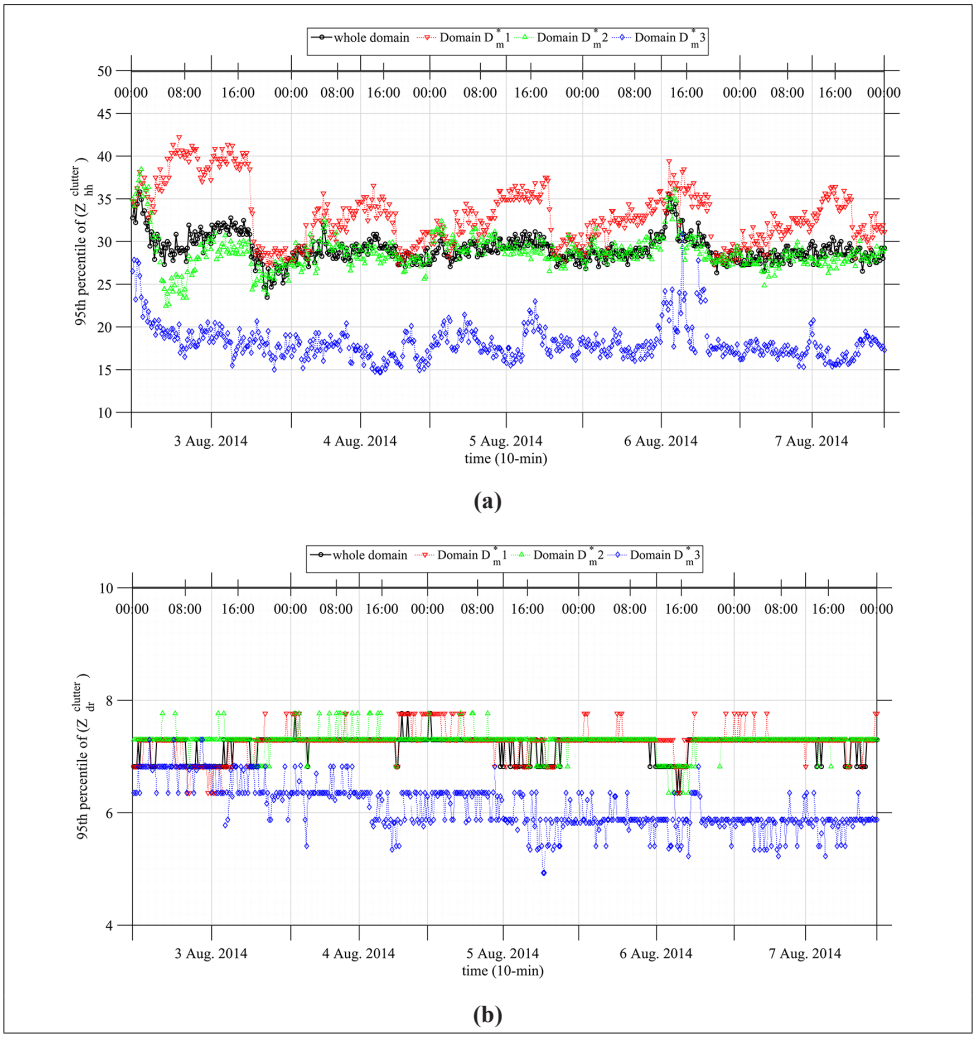

Figure 9 - Temporal trend in time of acquisition of the 95th percentile of the cumulative distribution for the co-polar reflectivity (a) and differential reflectivity (b).

From these tables, it emerges that the lowest standard deviation is found for domain D when considering Z_{dr} (look at the lowest standard deviation $s\left(\bar{Z}_{dr}^{D}\right)$ in Tab. 4), whereas in terms of Z_{hh} the lowest standard deviations are found for first sub-region domain, (look at the lowest values of $s\left(\bar{Z}_{hh}^{D_m^*1}\right)$ in Tab. 4). This result indicates that areas around the radar system, i.e. those in the domain are more suitable to calibrate the co-polar reflectivity, Z_{hh}, whereas the whole domain D can be efficiently used to calibrate the differential reflectivity Z_{dr} The comparison between Tables 3 and 4 highlighted that the standard deviations associated with the mean value statistical parameter (Tab. 3) are lower than those associated to the 95th percentile. Note that, considering that 1 dBZ and 0.1 dB are the typical limits for the estimated precision of the calibration techniques [Bringi and Chandrasekar, 2001], a fluctuation of the same amplitude makes unsuitable the 95th percentile for this purpose.

Table 3 - Standard deviations for the co-polar reflectivity and differential reflectivity of the ground-clutter sub-regions D_m^*1, D_m^*2, D_m^*3 and the whole clutter scenario D using the mean value statistical parameter. The clutter domain D is basically the dynamical clutter map for each instant within the training dataset as defined in Section "Ground-clutter analysis by region merging". The subdomains D_m^*1, D_m^*2, D_m^*3 are sub-regions not necessarily connected, output of the region merging algorithm that have more stable clutter PDFs inside it.

	3 Aug 2014		4 Aug 2014		5 Aug 2014		6 Aug 2014		7 Aug 2014	
	$s(\bar{Z}_{hh})$	$s(\bar{Z}_{dr})$	$s(\bar{Z}_{hh})$	$s(\bar{Z}_{dr})$	$s(\bar{Z}_{hh})$	$s(\bar{Z}_{dr})$	$s(\bar{Z}_{hh})$	$s(\bar{Z}_{dr})$	$s(\bar{Z}_{hh})$	$s(\bar{Z}_{dr})$
D	0.6570	**0.1324**	0.4196	**0.1111**	0.5372	**0.1156**	1.1517	**0.1207**	0.2611	**0.0940**
D_m^*1	**0.5958**	0.3881	**0.4111**	0.1858	**0.4981**	0.2772	**0.7883**	0.2388	**0.2457**	0.2127
D_m^*2	0.7036	0.1710	0.4852	0.1433	0.5140	0.1532	1.6153	0.1849	0.3346	0.1176
D_m^*3	0.7881	0.3215	0.5243	0.2485	0.7650	0.2355	1.1024	0.3281	0.5218	0.2477

Table 4 - Standard deviations for the co-polar reflectivity and differential reflectivity of the ground-clutter regions D_m^*1, D_m^*2, D_m^*3 and the whole clutter scenario D using the 95th percentile statistical parameter. The definitions of the domain D and sub-domains is in Table 3.

	3 Aug 2014		4 Aug 2014		5 Aug 2014		6 Aug 2014		7 Aug 2014	
	$s(95\bar{Z}_{hh})$	$s(95\bar{Z}_{dr})$	$s(95\bar{Z}_{hh})$	$s(95\bar{Z}_{dr})$	$s(95\bar{Z}_{hh})$	$s(95\bar{Z}_{dr})$	$s(95\bar{Z}_{hh})$	$s(95\bar{Z}_{dr})$	$s(95\bar{Z}_{hh})$	$s(95\bar{Z}_{dr})$
D	2.4634	0.2288	0.9551	0.1186	0.9676	0.2188	1.8041	0.2215	0.8128	0.1484
D_m^*1	4.7192	0.3043	2.3508	0.2187	2.6451	0.2645	2.8530	0.2177	1.9963	0.1640
D_m^*2	3.4633	0.1664	1.2742	0.1921	1.1570	0.1873	1.8552	0.2593	0.8419	0.0809
D_m^*3	2.3384	0.3105	1.3618	0.3284	1.4901	0.3563	2.6603	0.2531	1.0663	0.2221

One of the interesting aspects of this analysis is the possibility to use different domains to analyse the various radar observables, such as in this case. A deeper analysis of the considered dataset also shows that in the whole domain and in the sub-domain the trend of the standard deviation increases during the day and decreases during the night (see Fig. 8). This interesting aspect, more visible in the stable first sub-domain, D_m^*1 (Fig. 8a), can be due to ground-clutter induced by anomalous propagation occurring as a result of nocturnal radiative cooling [Moszkowicz et al., 1994]. Further future investigations will be useful to establish this tendency. Concerning the statistical parameter, the mean value of the probability distribution is preferable to the 95th percentile value being it much more variable (based on Tabs .4-5 and also on Figs. 8 and 9). This means that in the overall approach we can use Equation [9] applied to the three identified stable sub-domains $D = D_m^*j$.

Relative calibration results

The final result of the overall approach, illustrated in Figure 1, are listed in Table 5 in terms of relative calibration values for Z_{hh} and Z_{dr} and its uncertainty. These results are expressed as a temporal averages of the differences on sequential days following Equation [9]. Tab. 5 also

compares our results with the absolute receiver calibration value obtained by means of the Sun-monitoring approach [Holleman et al., 2010]. Note that the latter provides an absolute calibration as opposed to a relative calibration so that they should be carefully used by looking at the daily differences (and not as absolute values). For clarity, the absolute calibration gives an estimate of the value of the miscalibration whereas the relative calibration measures the loss of calibration in time as a differences between two temporal measurements. Table 5 shows the Sun absolute calibration (indicated as SAC), the Sun daily differences (indicated as Sun SDD) compared with the Ground-clutter daily differences (indicated as Clutter CDD). The starting value for the relative calibration on the first day (3 August 2014) is zero because 1-2 August 2014 have been used to train the Bayesian classifier (see section "Ground-clutter Bayesian classification"). From Table 5 we realize that the relative calibration values for the differential reflectivity have little temporal variations and this feature is confirmed by the absolute Sun monitoring values. The relative calibration values for the co-polar reflectivity have a much bigger variation and agree with the Sun monitoring. The residual error between Sun-interference and clutter-based calibration may be due to the miscalibration of the radar transmitting part, which is taken into account only in the ground-clutter based results. The Sun-interference calibration extracts only the radar receiver miscalibration because the system is considered as a passive monitoring of Sun radiation. On the other hand, the clutter-based calibration considers the whole system evaluating the sum of the transmitter and the receiver miscalibration.The reference works for the clutter-based relative calibration [Silberstein et al., 2008; Golbon-Haghighi et al., 2015; Wolff et al., 2015] focused their efforts in the evaluation of long temporal trend of calibration values obtained by using the whole clutter domain. The uncertainty on the estimated calibration values was not taken into account in this works. As a matter of fact the standard deviation of these daily temporal trend of the calibration values was guaranteed around 10 dB for the reflectivity.Then an important result of our statistical analysis for the clutter-based relative calibration is also the result in terms of uncertainty, as shown in Table 3. This uncertainty is computed as the standard deviation of daily temporal trend of the calibration values (see Figs. 8 and 9). The estimated uncertainty is not exceeding 1 dBZ and 0.1 dB for Z_{hh} and Z_{dr} respectively [Bringi and Chandrasekar, 2001]. These values are in agreement with upper limit needed for an accurate estimation of precipitation intensity and hydrometeors classification.

Table 5 - Absolute and relative calibrations for the co-polar reflectivity and for the differential reflectivity. All values in the table are in dB.

	3 Aug 2014		4 Aug 2014		5 Aug 2014		6 Aug 2014		7 Aug 2014	
	Z_{hh}	Z_{dr}	Z_{hh}	Z_{dr}	Z_{hh}	Z_{dr}	Z_{hh}	Z_{dr}	Z_{hh}	Z_{dr}
Clutter Daily Difference # = *CDD*	0	0	0.3511	-0.0568	0.6302	-0.0521	0.0581	0.0044	0.0581	-0.0854
Sun Daily Difference # = *SDD*	0	0	0.3154	0	0.5213	0.07	0	0	0	0
Sun Absolute Calibration # = *SAC*	0.0462	0.53	0.3616	0.53	0.8829	0.6080	0.8829	0.6080	0.8829	0.6080

Conclusions

This work has been devoted to the improvement of ground-clutter classification and clutter-based relative calibration monitoring, using a C-band polarimetric weather radar located in the complex orography of southern Italy. In the available literature there are several works presenting results on different weather-radar calibration techniques, but only few of them use ground-clutter echoes as calibration targets monitoring [Silberstein et al., 2008; Golbon-Haghighi et al., 2015; Wolff et al., 2015].

The main goal of this work has been to propose an overall self-consistent approach for clutter-based relative calibration including both a Bayesian radar-signal classifier and region-merging algorithm to objectively identify those radar grid-points affected by ground clutter with a more stable behaviour in terms of its temporal and spatial statistical features. Both classification and segmentation algorithmic steps have been discussed, showing potentials and limitations of the proposed methodology.

The results, based on a relatively limited dataset, show that a relative radar calibration can usefully exploit the identification of stable clutter sub-domains and the analysis of the daily mean value of co-polar and differential reflectivity. It is worth noting that the standard deviation, both for co-polar and differential reflectivity shows a diurnal cycle, a feature which might be exploited to better characterize clutter scenarios. A future development of this work will be focused on the enlargement of the available radar dataset and possibly extend the analysis to other C-band polarimetric radar systems. Moreover, the same overall approach could be further developed in order to include other polarimetric observables such as the co-polar correlation coefficient. Thus, we will be potentially able to obtain several estimates of calibration errors derived by each of the various polarimetric variables considered and then merge them all together (e.g. using a fuzzy logic approach) into a single diagnostic quality index of radar calibration which would represent an easier way to check the calibration status of the whole radar system.

Acknowledgements

Data have been kindly provided by DPC (Department of Italian Civil Protection). A special thank goes to Dr. Gianfranco Vulpiani (DPC, Italy) for helpful discussions. Radar data used are under the DPC data policy.

References

Alberoni P.P., Ferraris L., Marzano F. S., Nanni S., Pelosini R., Siccardi F. (2002) - *The Italian radar network: current status and future developments.* Proceedings of ERAD02, pp. 339-344.

Alku L., Moisseev D., Aittomaki T., Chandrasekar V. (2015) - *Identification and Suppression of Nonmeteorological Echoes Using Spectral Polarimetric Processing.* IEEE Transaction on Geoscience and Remote Sensing, 53 (7): 3628-3638. doi: http://dx.doi.org/10.1109/TGRS.2014.2380476.

Bringi V.N., Chandrasekar V. (2001) - *Polarimetric Doppler Weather Radar: Principles and Applications.* Cambridge University Press. doi: http://dx.doi.org/10.1017/CBO9780511541094.

Browning K.A. (1978) - *Meteorological applications of radar.* Reports on progress in physics, 41 (5): 761-806.

Falconi M.T., Vulpiani G., Montopoli M., Marzano F.S. (2015) - *C-Band Polarimetric Weather Radar Calibration using a fuzzy logic fusion of three techniques.* Proceedings of IGARSS 2015, pp. 5363-5366. doi: http://dx.doi.org/10.1109/IGARSS.2015.7327047.

Golbon-Haghighi M.-H., Zhang G. Li Y., Doviak R.J. (2016) - *Detection of Ground Clutter from Weather Radar Using a Dual-Polarization and Dual-Scan Method.* Atmosphere, 7 (6): 83. doi: http://dx.doi.org/10.3390/atmos7060083.

Gorgucci E., Scarchilli G., Chandrasekar V. (1999) - *A procedure to calibrate multiparameter weather radar using properties of the rain medium.* IEEE Transaction on Geoscience and Remote Sensing, 37 (1): 269-276. doi: http://dx.doi.org/10.1109/36.739161.

Haykin S., Deng C. (1991) - *Classification of radar clutter using neural networks.* IEEE Transactions on Neural Networks, 2 (6): 589-600. doi: http://dx.doi.org/10.1109/72.97936.

Haykin S., Stehwien W., Deng C., Weber P., Mann R. (1991) - *Classification of radar clutter in an air traffic control environment.* Proceedings of IEEE, 79 (6): 742-772. doi: http://dx.doi.org/10.1109/72.97936.

Holleman I., Huuskonen A., Kurri M., Beekhuis H. (2010) - *Operational monitoring of weather radar receiving chain using the Sun.* Journal of Atmospheric and Oceanic Technology, 27 (1): 159-166. doi: 10.1175/2009JTECHA1213.1.

Hubbert J.C., Dixon M., Ellis S.M., Meymaris G. (2009a) - *Weather Radar Ground-clutter. Part I: Identification, Modeling, and Simulation.* Journal of Atmospheric and Oceanic Technology, 26 (7): 1165-1185. doi: http://dx.doi.org/10.1175/2009JTECHA1159.1.

Hubbert J.C., Dixon M., Ellis S.M., Meymaris G. (2009b) - *Weather radar ground-clutter. Part II: Real-time identification and filtering.* ournal of Atmospheric and Oceanic Technology, 26 (7): 1181-1197. doi: http://dx.doi.org/10.1175/2009JTECHA1160.1.

Ice R.L., Heck J.G., Cunningham J.G., Zittel W.D. (2014) - *Challenges of polarimetric weather radar.* Proceedinds of ERAD 2014 , vol. ID-117.

Jakubiak A., Arabas J., Grabczak K., Radomski D., Swiderski J.F. (1997) - *Radar clutter classification using Kohonen neural network.* IEEE conference publication, pp. 185-188. doi: http://dx.doi.org/10.1049/cp:19971658.

Kotz S., Nadarajah S. (2000) - *Extreme value distributions: theory and applications.* World Scientific.

Lee H., Kim E.K., Kim S. (2015) - *Anomalous propagation echo detection using artificial neural network and doppler velocity features.* IEEE International Conference on Advanced Intelligent Mechatronics (AIM), pp. 377- 381. doi: http://dx.doi.org/10.1109/AIM.2015.7222561.

Moszkowicz S., Ciach G. J., Krajewski W.F. (1994) - *Statistical Detection of Anomalous Propagation in Radar Reflectivity Patterns.* ournal of Atmospheric and Oceanic Technology, 11: 1026-1034. doi: http://dx.doi.org/10.1175/1520-0426(1994)011<1026:SDOAPI>2.0.CO;2.

Nock R., Nielsen F. (2004) - *Statistical region merging.* IEEE Transactions on Pattern Analysis and Machine Intelligence, 26 (11): 1452-1458. doi: http://dx.doi.org/10.1109/TPAMI.2004.110.

Passarelli R.E., Romanik P., Geotis S.G., Siggia A.D. (1981) - *Ground-clutter rejection in the frequency domain (for radar meteorology applications).* Conference on Radar Meteorology, 20th, Boston, MA, pp. 295-300.

Rico-Ramirez M.A., Cluckie I.D. (2008) - *Classification of Ground-clutter and Anomalous Propagation Using Dual-Polarization Weather Radar.* IEEE Transaction on Geoscience and Remote Sensing, 46 (7): 1892-1904. doi: http://dx.doi.org/10.1109/TGRS.2008.916979.

Ryzhkov V.R., Giangrande S.E., Melnikov V.M., Schuur T.J. (2005) - *Calibration issues of dual-polarization radar measurements.* Journal of Atmospheric and Oceanic Technology, 22: 1138-1155. doi: http://dx.doi.org/10.1175/JTECH1772.1.

Saltikoff E., Cho Y.N.J., Tristant P., Huuskonen A., Allmon L., Cook R., Becker E., Joe P. (2016) - *The Threat to Weather Radars by Wireless Technology.* Bulletin of the American Meteorological Society, 97 (7): 1159-1167. doi: http://dx.doi.org/10.1175/BAMS-D-15-00048.1.

Schaefer J.T. (1990) - *The critical success index as an indicator of warning skill.* Weather and Forecasting, 5 (4): 570-575. doi: http://dx.doi.org/10.1175/1520-0434(1990)005%3C0570:TCSIAA%3E2.0.CO;2.

Silberstein D.S., Wolff D.B., Marks D.A., Atlas D., Pippitt J.L. (2008) - *Ground Clutter as a Monitor of Radar Stability at Kwajalein, RMI.* Journal of Atmospheric and Oceanic Technology, 25 (11): 2037-2045. doi: http://dx.doi.org/10.1175/2008JTECHA1063.1.

Steiner M., Smith J.A. (2002) - *Use of three-dimensional reflectivity structure for automated detection and removal of nonprecipitating echoes in radar data.* Journal of Atmospheric and Oceanic Technology, 19 (5): 673-686. doi: http://dx.doi.org/10.1175/1520-0426(2002)019<0673:UOTDRS>2.0.CO;2.

Vaccarono M., Bechini R, Chandrasekar V., Cremonini R., Cassardo C. (2016) - *An integrated approach to monitor the calibration stability of operational dual-polarization radar.* Atmospheric Measurement Techniques Discussions, pp. 1-31. doi: http://dx.doi.org/10.5194/amt-2016-36.

Vulpiani G., Montopoli M., Passeri L.D., Gioia A.G., Giordano P., Marzano F.S. (2012) - *On the use of dual-polarized c-band radar for operational rainfall retrieval in mountainous areas.* Journal of Applied Meteorology and Climatology, 51 (2): 405-425. doi: http://dx.doi.org/10.1175/JAMC-D-10-05024.1.

Wolff D.B., Marks D.A., Petersen W.A. (2015) - *General Application of the Relative Calibration Adjustment (RCA) Technique for Monitoring and Correcting Radar Reflectivity Calibration.* Journal of Atmospheric and Oceanic Technology, 32 (3): 496-506. doi: http://dx.doi.org/10.1175/JTECH-D-13-00185.1.